Available online at www.sciencedirect.com
SCIENCE DIRECT®
Journal of Power Sources xxx (2005) xxx–xxx
JOURNAL OF POWER SOURCES
www.elsevier.com/locate/jpowsour

State-of-charge determination of lead-acid batteries using wire-wound coils

Ian R. Hill [a,*], Ed E. Andrukaitis [b]

[a] *Institute for Chemical Process and Environmental Technology, National Research Council of Canada, Ottawa, Ont., Canada K1A 0R6*
[b] *Defence Research and Development Branch, National Defence Headquarters, 305 Rideau Street, Ottawa, Ont., Canada K1A 0K2*

Abstract

Non-intrusive monitoring of the state-of-charge of sealed lead-acid batteries using wire-wound coils is described. Coils were attached to the plastic case of the batteries, adjacent to the negative end plate, and excited using ac current at 10 kHz. As the batteries were cycled, the inductance of the coils tracked the change in metallic content of the end plates. Data is presented for different discharge rates and temperatures. A variation of the technique is also described that uses less expensive equipment to measure the voltage drop across the coil, rather than inductance.

Keywords: Lead-acid; State-of-charge; Inductance; Coil

1. Introduction

The state-of-charge (SOC) of lead-acid batteries is of particular interest in applications that involve deep discharging, such as electric vehicles, silent watch and submarine propulsion. Traditionally, the SOC is estimated from the discharging voltage and current of the battery using algorithms, or from using sensors inside the battery. However, a reliable way of probing the SOC external to the battery would be preferable. Several patents have been published during recent years concerning the use of the inductance of wire-wound coils to monitor the state-of-charge of lead-acid batteries [1–3]. In a previous publication [4], we presented inductance data from flooded lead-acid batteries and showed that it also was important to monitor the battery temperature in order to correct the inductance data for temperature changes inside the battery. It was found to be necessary to recalibrate the inductance profile every 10 cycles because of drifting of the background signal due to changes in the electrode structure, especially during earlier cycles. Complete details of the technique can be found in reference [4], but the basic principles are as follows. A coil is firmly attached to the battery case such that its windings are parallel to the surface of the end plate of the battery. The end plates of a lead-acid battery are normally the negative, metallic lead electrodes. When an alternating current is applied to the coil, it generates a magnetic field that propagates along the axis of the coil winding into the battery. This alternating magnetic field can propagate through an insulator but will be absorbed by a conductor, such as a metal electrode. The energy lost from the magnetic field of the coil to the conductor, can be detected via the drop in inductance of the coil compared with that measured in air. The alternating magnetic field generates eddy currents in the conductor that mirror the current flow in the coil and which set up an opposing alternating magnetic field. In this way, the intrinsic inductance of the coil is reduced in the proximity of the metal electrode—the coil is being used as a metal detector. This technique should be considered for applications with rechargeable batteries that have relatively flat discharge curves and especially for sealed or gelled-electrolyte systems.

During discharging of a lead-acid battery, the lead in the negative electrode active material is converted to lead sulphate, so the total metallic content of the electrode is lowered. The alternating magnetic field does not interact with lead sulphate, so the flux of eddy currents is reduced, resulting in

* Corresponding author. Tel.: +1 613 998 6814; fax: +1 613 991 2384.
E-mail address: ian.hill@nrc-cnrc.gc.ca (I.R. Hill).

0378-7753/$ – see front matter.
doi:10.1016/j.jpowsour.2005.07.019

an increase in the measured inductance of the coil. Therefore, the coil inductance changes with the state-of-charge (SOC) of the negative electrode. The positive electrode active material changes from lead dioxide to lead sulphate during discharging, so this electrode will not affect the coil inductance during cycling. The coil needs to be as close as possible to the electrode and only a small range of frequencies has been found to be useful (5–20 kHz) and we typically use 10 kHz. Absorption of the electromagnetic field by a metal follows the relationship $\delta = (\pi\mu\sigma f)^{-1/2}$, where δ represents the depth at which the field is attenuated by $1/e$, or 63%, and is termed the skin depth. Here, μ is the permeability of the material (which is equal to $4\pi \times 10^7$ H m^{-1} for non-ferromagnetic materials such as lead); σ is the conductivity; f is the frequency of the oscillating field. For lead, the skin depth was calculated to be 2.3 mm at 10 kHz, which is the same order of magnitude as the thickness of lead-acid battery plates. The changes in inductance are not quantitative by themselves because the distance between the coil and the lead electrode is not known. Rather, the battery needs to be cycled in order to generate a calibration curve relating the inductance changes to the true SOC. Because the coil is being used to detect metal, it is apparent that the batteries being considered here should have non-metallic cases. This coil technique is a new application of eddy current analysis, which is in widespread use in the aerospace industry for detecting cracks or corrosion in the metal skin of aircraft. However, in the present application, the coils being used have much larger diameter, in order to sense the average composition of the electrode.

2. Experimental

Two sizes of coil were used in the work reported here, which were 35 mm diameter and were hand wound onto polycarbonate spools. The ferrite pot cores and polycarbonate spools were obtained from ELNA Ferrite Labs Inc., Woodstock, New York. The ferrite cores were made from a mixed MnZn or NiZn ferrite and had initial permeabilities of 2300 ± 20%, with an optimum frequency range below 300 kHz. The coils that were wound using 34 gauge, lacquered, copper wire typically had an inductance of around 45 mH, which increased to 175 mH when placed inside the pot core. The coil that was wound using 28 gauge wire had an inductance of 0.68 mH and was used without a core. Impedance data were acquired using a Hewlett-Packard HP 4192A LF Impedance Analyser, which has an oscillator level in the range of 5 mV to 1.1 V. Inductance (L) was measured as [inductive reactance]/[angular frequency], or X_L/ω. The 12 V lead-acid batteries used were 12FV120 Armasafe Plus, deep cycle batteries from Hawker Ltd., Manchester, UK. The batteries were cycled using a Digatron Electronic Universal Battery Tester (UBT1-50). Depending on the discharge rate, measurements were taken every 2 or 5 min during battery cycling, using a controlling programme written in Labview 4.0. The external temperature of the cell that was being monitored by the coil was sampled using a thermocouple. Voltages and currents were measured using Fluke 8840A and Hewlett-Packard 34401 A multimeters. A Wavetek 75 A random waveform generator was used to drive the 0.684 mH coil. A Thermotron S-8 environmental chamber was used to equilibrate the batteries at different temperatures.

3. Results and discussion

3.1. Inductance behaviour during battery cycling

The valve-regulated 12FV120 Hawker Armasafe Plus battery has recently been placed into service by the Canadian Armed Forces, replacing an earlier flooded version (6TLFP). Because the battery is sealed, the specific gravity of the electrolyte cannot be used to estimate the SOC, which also applies to gelled electrolyte batteries. Having already established the feasibility of the coil technique with the flooded electrolyte version of the battery [4], it was logical to apply the technique to a valve-regulated lead-acid (VRLA) battery. The 12FV120 battery has a nominal capacity of 110 Ah at the $C/10$ rate and a recommended charging voltage of 14.25 ± 0.25 V. Fig. 1A shows the voltage and current profiles during some early cycles of this battery; the battery was being charged for 26 h to 14.25 V with a limiting current of 10 A. Fig. 1B shows the corresponding changes in the inductance of the attached coil and the temperature of the cell being sampled, measured externally by thermocouple. During discharging, the measured inductance increases as the quantity of lead in the negative plate decreases. With charging, the inductance falls smoothly until just before the voltage reaches the 14.25 V limit: after this point, the temperature begins to increase at a faster rate and a shoulder is seen in the inductance profile.

In our earlier paper [4], we showed how the inductance data need to be corrected for internal changes in temperature of the battery during charging and discharging. The correction factor of the present battery (in mH °C^{-1}) was determined by placing battery and attached coil inside an environmental chamber and varying the temperatures between +20 °C and −20 °C, using increments of 10 °C. Because of the high thermal mass of the battery and the low thermal conductivity plastic case, it took 24 h for the signal to stabilize at each temperature. A plot of inductance versus temperature was almost linear over this range and was taken to be linear over the 5–8 °C excursions seen during cycling. The correction factor was determined to be 0.0350 mH °C^{-1}. Fig. 1B compares the experimentally recorded inductance with that corrected for the temperature variation. It can be seen that the small hump observed towards the end of the 10 A part of charging has been mostly removed. The reason that the hump was not completely removed is attributed to slow heat transfer through the plastic battery case. This was not a problem in earlier work using vented batteries because the thermocouple was placed inside the cell. This exothermic reaction takes place at the surface of the active material of the negative electrode, so the

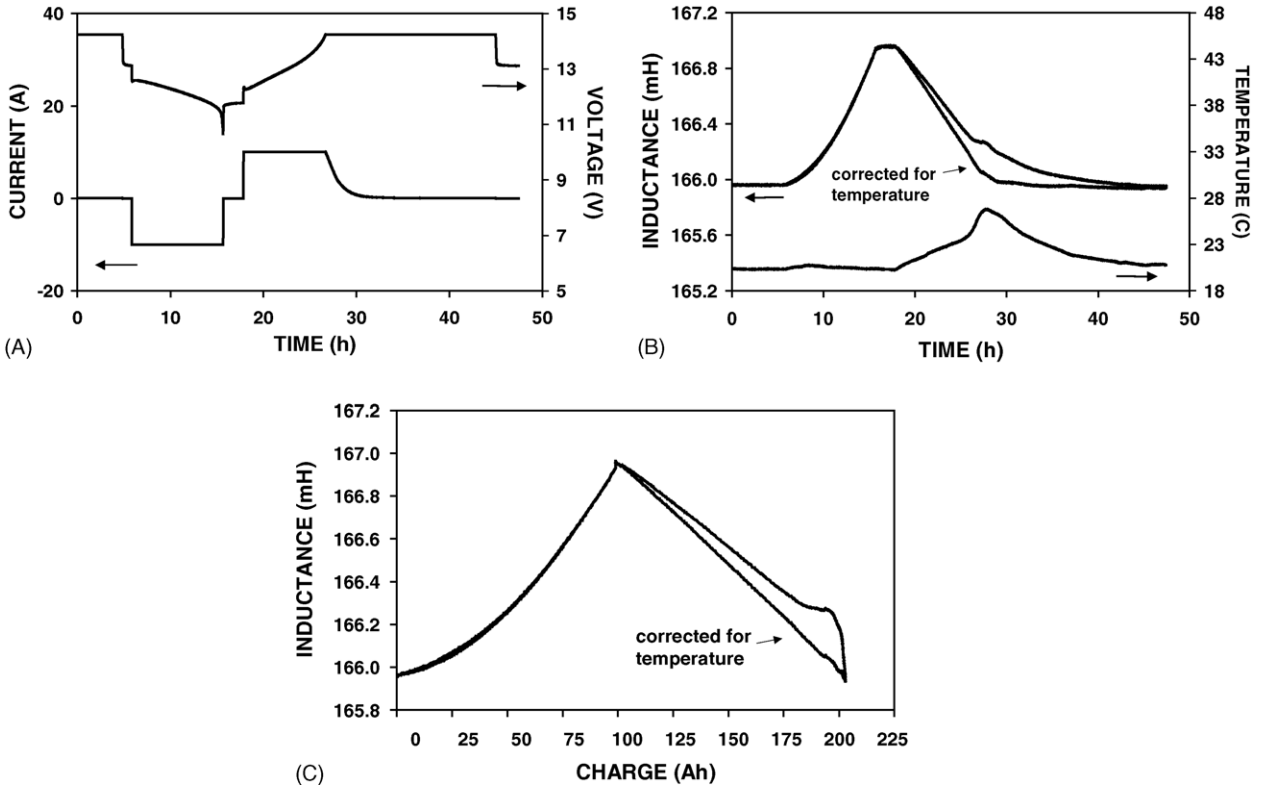

Fig. 1. Cycling behaviour of a 12 V, Hawker Armasafe, VRLA battery. (A) Voltage and current profiles (charging was for 28 h at 10 A to 14.25 V, and discharging at 10 A to 10.5 V). (B) The corresponding changes in coil inductance at the negative end-plate of one of the cells, plus the inductance after correction for temperature changes inside the battery. (C) The inductance data for one of the cycles plotted against the absolute value of the charge passed (all inductance data is for 10 kHz unless stated otherwise).

inductance data will reflect the temperature of the negative electrode. It is useful to plot the inductance changes versus the charge passed, as is done in Fig. 1C (integrated absolute value of the charge). Here, the corrected profile for charging looks almost linear and is not the same shape as the profile for discharging. The discharging profile mainly differs over the first 20% of the discharge. The smaller changes probably reflect initial discharging being concentrated on the far side of the end plate (remote from the coil) closer to the positive electrode, resulting in a weaker effect on the coil inductance. One factor affecting this is the slow diffusion rate of the large HSO_4^- ions, which are consumed in the discharge reaction, such that there is likely to be a lower concentration of HSO_4^- ions towards the near side of the end plate. The more linear shape of the charging profile also reflects the fact that the charging process is more evenly distributed throughout the electrode because of the high diffusion rate of H^+ ions, which are consumed in that reaction. The charging profile can also be corrected for the loss of charge to heat, as outlined in reference [4]. This correction only affects the profile near the end-of-charge and does not have a significant impact on its shape.

Fig. 2A shows the inductance profiles of eight consecutive cycles, along with the discharge capacities. Here, the charging time was limited to 12 h, so the battery was not completely recharged. It can be seen that the inductance profiles are not exactly reproducible from one cycle to the next but, nevertheless, the SOC can be estimated to within ±10% for the steeply sloping part of the profile of any given discharge, relative to the profile of the first discharge. However, the inductance does not change much during the first 20% of the discharge, so the errors are much higher in that region. Fig. 2B compares the inductance profiles for the first and last discharges shown in Fig. 2A. The curves are still generally the same shape but they deviate at high SOC and, because this part of the curves is relatively flat, there is a much larger error in estimating the SOC in this region. With all of the lead-acid batteries that we have investigated using this inductance technique there has always been a significant drift in the background signal to higher inductance, particularly over the first 20 cycles as the electrode microstructure progressively changes to an equilibrium value. The negative electrode has a primary skeletal structure of lead, which serves as a current collector and a support for the secondary structure of energetic material [5,6]. The active mass swells and becomes more porous during cycling. The lead crystals grow larger during these early cycles and the BET surface area falls. The result is a loss of contact between some branches of the skeleton, so the resistance increases. It is this increased resistance that results in drifting of the inductance background to higher values during early cycles.

A change in shape of the inductance curve for discharging also occurs during early cycles. Fig. 3A compares the

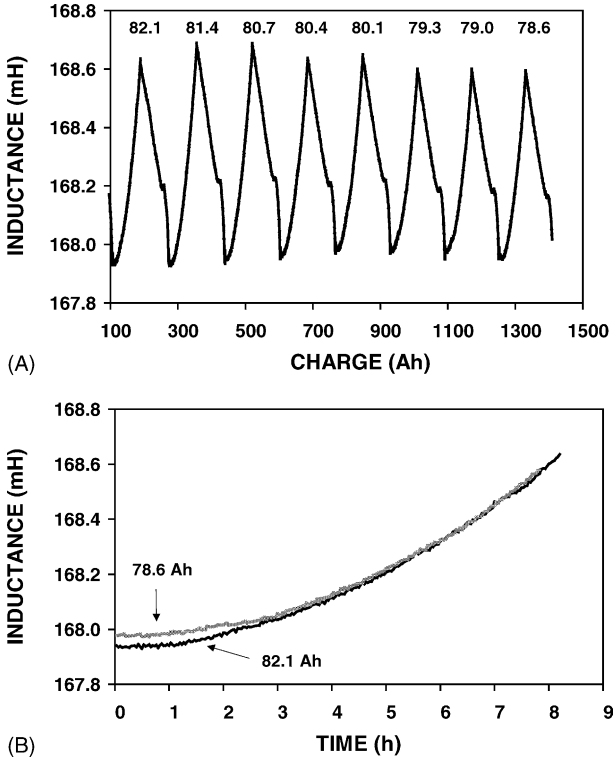

Fig. 2. (A) Compares the inductance profiles for eight consecutive cycles, with charging time limited to 12 h (20 A, 14.25 V). The discharge capacities are included above the curves. The profiles are not exactly reproducible from cycle to cycle, but can still be used to estimate the SOC. (B) Compares the discharge profiles of the first and last cycles of Fig. 2A. Deviation is seen at high SOC.

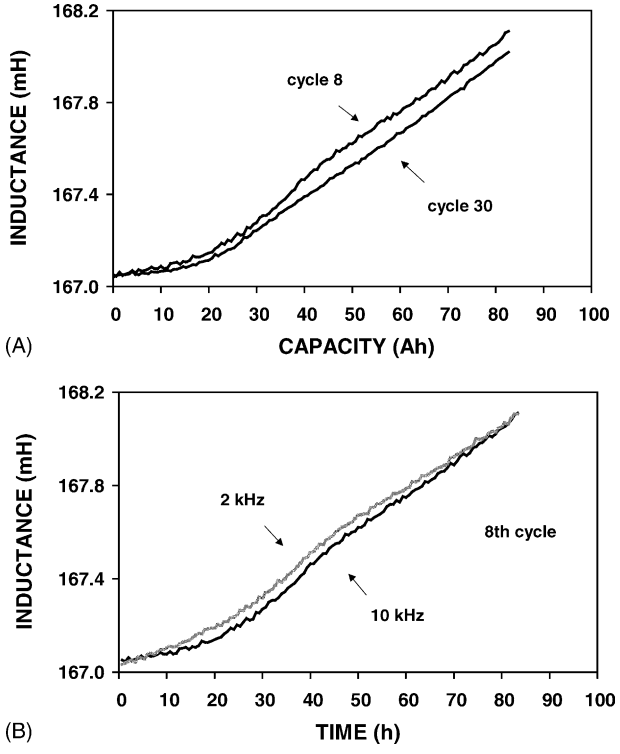

Fig. 3. (A) Compares the inductance profiles for 10 A discharging on cycles 8 and 30. There has clearly been a change in shape, which always occurs during the first 20 cycles as the electrodes fully form. (B) Compares the shapes profiles on the eighth cycle, using two frequencies for the coil (the 2 kHz profile has been scaled up for the comparison). The lower frequency samples to a greater distance away from the coil.

inductance discharge profiles of the 8th and 30th cycles. The eighth cycle shows a greater sensitivity to the discharge over the first half of the discharge, then the curves are parallel for the second half. These changes are difficult to explain but must reflect the structural changes that have taken place in the electrode. Fig. 3B compares the eighth cycle using 2 and 10 kHz ac current. The magnetic field generated at 2 kHz has a greater sampling depth into the electrode than that at 10 kHz. As mentioned earlier, initial reaction is expected to be weighted towards the positive electrode side of the end plate. Therefore, the 2 kHz field should be more sensitive to initial discharging, as is seen to be the case with the steeper slope of the 2 kHz curve at short discharge times. The fact that the 10 kHz curve is very flat during initial discharging indicates that there is little reaction towards the outer surface of the end plate.

3.2. Intermittent discharging

Fig. 4 shows the voltage profile for an intermittent discharge carried out at 10 A, using a repetition of 2 h on discharge then 2 h at rest. The inductance signal is seen to be constant at open circuit, as expected. In contrast, the voltage takes some time to recover to a steady value at open circuit. Therefore, the inductance measurement is useful for monitoring intermittent discharges without being connected to the battery circuit.

3.3. Discharging at different rates

Fig. 5A compares the inductance curves obtained from discharging at 10, 20 and 50 A, as well as from a partial discharge at 250 A. The curves are all the same general shape with the changes in inductance being smaller for the first 10–20% of

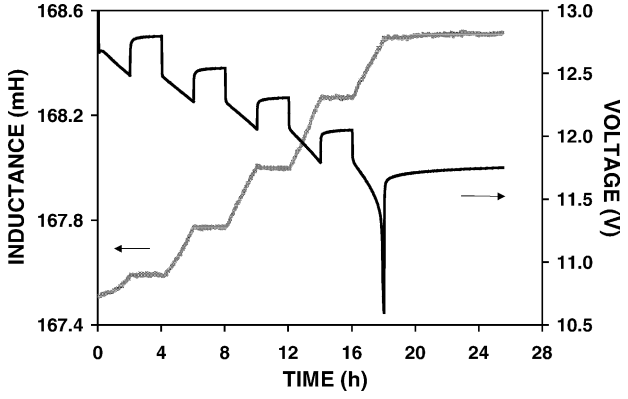

Fig. 4. The battery was subjected to an intermittent discharge at 10 A, using 2 h on and 2 h rest. The inductance signal is seen to be flat during the rest periods, as expected.

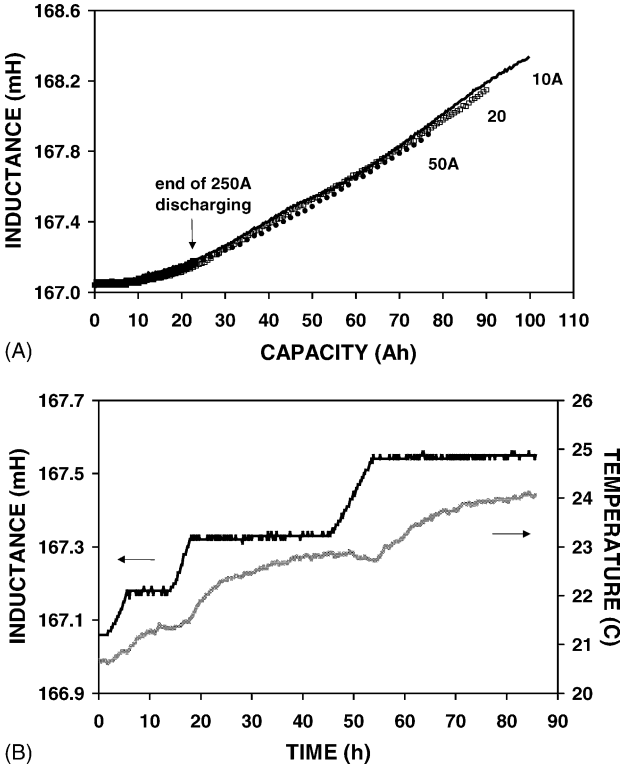

Fig. 5. (A) The inductance curves for discharging at different rates are compared and are seen to be almost superimposeable. The 250 A discharge was terminated after 5 min. (B) The inductance curve for two 5-min 250 A discharges and then a 125 A discharge for 10 min. The inductance cannot be corrected for temperature in this case because of the high lag time for sensing the temperature outside the case.

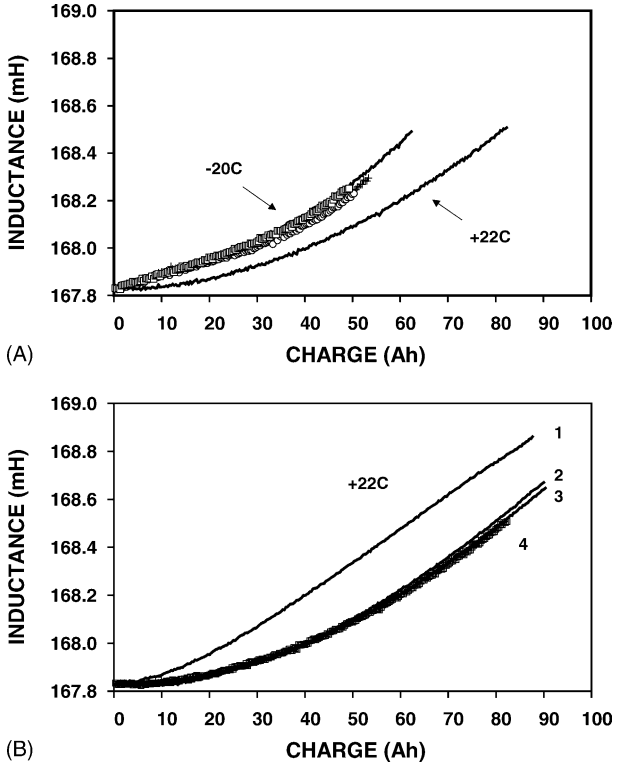

Fig. 6. (A) Compares the inductance profiles for discharging, first at room temperature and then at −20 °C, at which four cycles were performed. The profiles at −20 °C are all closely similar and quite different from that at room temperature. (B) Shows the first three cycles performed at room temperature following the −20 °C cycling (numbered 1–3) and compares them with the last cycle before the low temperature cycling (4). The first discharge has a profile similar to that at −20 °C, but the profiles relax back to the original shape (the backgrounds have been adjusted to match each other at the origin).

discharging and then increasing. Although the plots are nearly superimposeable, the inductance curve for 50 A is always to lower inductance of that for 10 A. This change reflects the discharge reaction occurring, on an average, further away from the coil at the 50 A rate. The 5-min, 250 A discharge resulted in the battery temperature rising by only 0.7 °C, but most of this temperature rise was detected after the discharge had finished, because of the slow thermal diffusion rate through the plastic battery case. The actual temperature at the negative electrode during discharging is not known so the inductance curve has not been corrected for temperature; nevertheless, the inductance curve tracks the other three closely. Fig. 5B shows the inductance curve for a discharge that consisted of two 250 A discharges for 5 min followed by one at 125 A for 10 min. The measured battery temperature is also included in the figure and can be seen to be of no use for correcting the data. The temperature actually at the negative electrode is apparently steady during the open circuit stands, in-between discharges, because the inductance reading is constant.

3.4. Discharging at different temperatures

Fig. 6A compares the inductance curve of a 20 A discharge performed at room temperature with those of the four proceeding cycles that were performed at −20 °C. The discharge curves have been corrected for temperature and it can be seen that the inductance curves at −20 °C are quite different from that at room temperature. The shape of the curves at −20 °C can be seen to remain relatively constant between cycles. The changes at −20 °C reflect a larger increase in resistance of the electrode as discharging progresses. This is to be expected because the resistance of metallic lead is lower at reduced temperatures, so the loss of metal has a larger effect on the inductance as discharging proceeds. The inductance at short discharge times is particularly different and appears to indicate that discharging is occurring, on average, closer to the coil at −20 °C, than at room temperature. One can speculate that this is because the micropores on the far side of the end plate (remote from the coil) are not as accessible at low temperatures and that larger pores surfaces throughout the electrode structure take part in the reaction at an earlier stage, so that, on an average, reaction is closer to the coil. Nevertheless, the total change in inductance for the first discharge at −20 °C is similar to that at +22 °C, so that the inductance values at −20 °C could be used to estimate a percentage SOC, as opposed to ampere-hour capacity.

Fig. 6B compares the inductance curves for discharging of the first three room temperature cycles following the −20 °C

cycles (labelled 1–3), plus the last room temperature discharge prior to the low temperature cycles (labelled 4). Curve 1 is very different from the other three and is similar to those that were obtained at −20 °C. This is in spite of the fact that the battery had been recharged at room temperature. The second discharge (2) was closer to the curve obtained prior to the low temperature cycles (4) and the third discharge (3) was the same shape as curve 4. Therefore, the negative electrode properties involving structure, resistance and porosity, as sampled by the inductance technique, had taken three cycles at room temperature to recover to their prior state. The exact nature of these changes is not known but one can speculate that the skeletal structure of the negative electrode active material suffered minor damage by the temperature change such that contact was lost between some branches, resulting in a higher resistance, but that contact was re-established with further cycling. At the same time, it is also possible that there is less reactive material that is partially blocking pores close to the negative electrode, which have been removed during further cycling. However, the data show that large errors can be introduced into the inductance measurement technique by varying the temperature substantially. It is apparent that the inductance technique for a battery will need to be calibrated for different temperatures, if accurate ampere-hour estimations are to be made. On the other hand it is nevertheless of interest that the inductance measurements are tracking changes in the negative electrode structure.

3.5. Effect of capacity degradation on inductance signal

Fig. 7A shows the inductance data for cycling the battery after 100 cycles and under conditions where it was being consistently undercharged. Charging was for 12 h at 10 A, 14.25 V and 101.5% of the discharge capacity was returned. The discharge capacities are listed at the top of the figure. The inductance curves for discharging can be seen to be falling in magnitude in parallel with the capacity. The interesting point about this data is that the falling values reflect a lower resistance in the electrode and, by inference, a higher metallic content, at all states-of-charge. The coils are 35 mm diameter, so the induced eddy currents traverse approximately 100 mm of the electrode interior and will not be sensitive to any possible electrically isolated crystals of metallic lead. Under these conditions, estimation of the SOC of later cycles using the first discharge in Fig. 7A is obviously very inaccurate. Fig. 7B compares the profiles of the first and last discharges of Fig. 7A. The last discharge needed to be shifted to the right to match the first discharge, so the profiles do not match at either the start or the end of discharge. This is not unexpected because the coils are only measuring a relative change in inductance and there is still unused active material present at the end of discharge. The falling trend in the inductance background reflects a lower resistance in the electrode and is counter intuitive. A possible explanation is that the lead crystals in the secondary structure of energetic material are growing larger and are contributing more to the conductivity of the electrode. In the immediately following cycles, the battery was charged for 24 h using a higher voltage limit of 14.6 V. The capacity recovered and the inductance data followed the reverse trend with the background signal rising and the profile returned to its previous shape. Therefore, the inductance data are relatively stable provided that the battery is completely recharged.

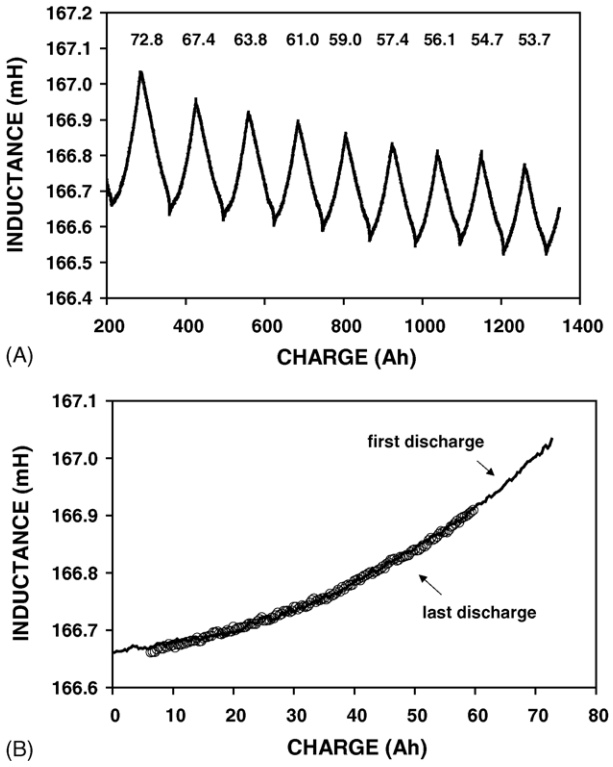

Fig. 7. (A) The effect that undercharging has on both the discharge capacity and the inductance signal. (B) A comparison of the shapes of the first and last discharge profiles from the data shown in (A)

3.6. Measurement of battery SOC using voltage drop across the coil

A major drawback with using inductance to monitor the SOC of lead-acid batteries is the high cost of the equipment needed for automatically monitoring the small changes in inductance during cycling. The equipment used for the above work was a computer controlled Frequency Response Analyser and several multimeters. The cost of a FRA is of the order of US$ 30,000 so a less expensive method of monitoring the coil-lead interaction is needed if the technique is ever to be used in the field. The alternative method that we adopted was to measure the voltage drop across the coil. This required the use of a high precision multimeter and an Arbitrary Waveform Generator (total cost US$ 3500). An appropriate 10 kHz waveform was needed that was sensitive to changes in the lead electrode. After some tests using different coils and waveforms, the eventual choice was a square wave of amplitude 5 V_{pp} coupled with a low inductance coil

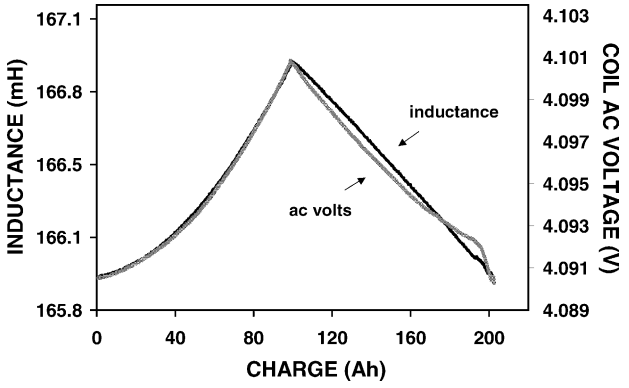

Fig. 8. The inductance profile of one cycle is compared with the ac voltage drop measured across a second coil. The second coil was excited using a 10 kHz square wave. The discharge curves can be seen to be the same shape.

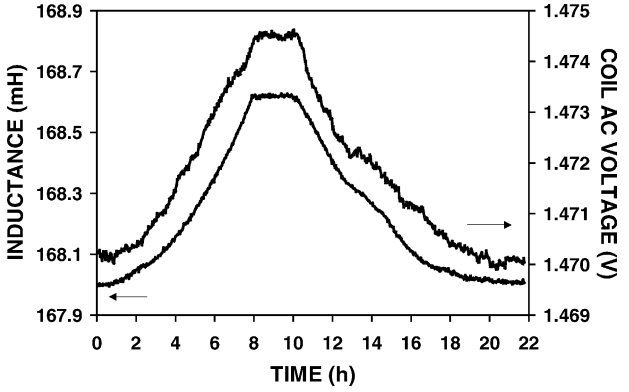

Fig. 10. The inductance profile of one cycle is compared with ac voltage data obtained using a dc power supply, a power transistor and a timer chip to drive the coil. This simple circuit is clearly inferior to using an arbitrary waveform generator to drive the coil.

(0.68 mH). This coil converted the 10 kHz square pulses into an exponential saw-tooth form and the height and shape of these were observed to be sensitive to metal content, with the aid of an oscilloscope. A battery was then cycled with two different coils attached to it: one for the usual inductance measurements and the other for the ac voltage measurement. In order to avoid possible interference, the coils were attached to separate cells in the battery. Fig. 8 compares the inductance and ac voltage profiles for a typical cycle at 10 A. Both curves have been corrected for temperature and the discharge portions of the curve can be seen to be closely similar in shape. The recharging portions are not as similar and the reason for this is not yet understood.

Fig. 9 compares the inductance and ac voltage signals from the battery as it was cooled down from +20 to −20 °C in increments of 10 °C, with the battery left at each temperature for 24 h. The battery was then subjected to four cycles at −20 °C, with the charging time limited to 18 h. It is apparent that the ac voltage measurements are not as sensitive to temperature as inductance is. The calibration curve for ac voltage coil versus temperature was linear with a slope of 9.5×10^{-5} V °C^{-1}. Because there is very little temperature change during a low rate discharge (C/10) of the battery, temperature correction of the inductance or ac voltage is not significant at room temperature. However, if a battery monitoring system is to be employed that includes this inductance SOC technique, the battery temperatures would be monitored anyway.

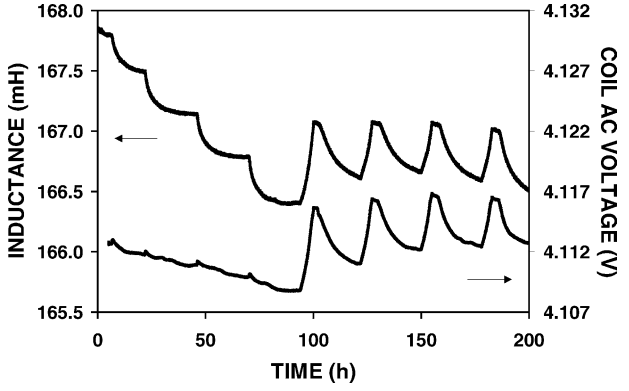

Fig. 9. A comparison of the inductance and ac voltage profiles from the two coils when the battery temperature was progressively lowered to −20 °C and four cycles performed at that temperature. The ac voltage is clearly less sensitive to temperature, so those profiles do not need to be corrected for small temperature changes during cycling.

Following the success of using the ac voltage of a coil to measure the SOC, it was decided to try and build a simple circuit to replace the arbitrary waveform generator using commonly available power transistors and timers. The circuit used a timer chip (#555) to help generate a 10 kHz square wave, which was inputted to a power transistor (P41C) that was used to drive the coil. The circuit was enclosed in a metal box for shielding and the power transistor was attached to a water-cooled thermal sink. A dc power supply (HP6291A) was used to power the circuit. Fig. 10 compares the inductance and ac voltage profiles for one cycle. The noise level of the ac voltage profile can be seen to be high. However, the data demonstrate that the SOC can be measured in this way using basic electronic components, so it may be possible to build a practical device using optimised components. In our particular case, the dc power supply that was used cost the same as the arbitrary waveform generator, so there was no benefit from using the homemade circuit. However, a less expensive power supply could be utilised, such as another battery in the case of monitoring a bank of large batteries.

4. Conclusions

Measurement of the inductance of wire-wound coils, using ac current in the frequency range 10 kHz, was found to be successful for non-intrusively monitoring the state-of-charge of sealed lead acid batteries. The battery–coil combination needs to be calibrated by performing complete discharge

cycles and the inductance signal needs to be corrected for temperature variations within the battery. The accuracy of the technique is affected by whether the battery is fully recharged and whether it has been subject to major temperature excursions. In either case, the signal relaxes back to the original values following further cycling under normal conditions. This coil technique should be particularly useful for monitoring the state-of-charge of sealed or gelled-electrolyte lead acid batteries and also for identifying the end-of-charge of the negative electrode. The inductance curves obtained during and following low temperature cycling are interesting because structural changes in the negative end plates were being monitored. Further work is required in order to confirm the present results and their interpretation, plus to determine the practicality of the technique in the field. The batteries discussed in the present paper are still being cycled.

Acknowledgements

The authors would like to thank Van Luong and Giulio Torlone of the National Research Council Canada for invaluable technical assistance.

References

[1] P.R. Stevenson, US Patent No. 5,093,624 (1992).
[2] D. Limuti, J.M. Ross, T.L. Churchill, US Patent No. 5,132,626 (1992).
[3] J.F. Beutler, B.J. Burreson, W.A. van Schalkwijk, D.F. Flagg, G.A. Kromholtz, J.J. Green, US Patent No. 5,537,042 (1996).
[4] I.R. Hill, E.E. Andrukaitis, J. Power Sources 103 (2001) 98–112.
[5] D. Pavlov, E. Bashtavelova, V. Iliev, Proc. Symp. Advances in Lead Acid Batteries, The Electrochemical Society, Pennington, NJ, USA, 1984, p. 16.
[6] A. Cooper, J. Power Sources 107 (2002) 245–272.